



# OPEN Starvation-induced HBP metabolic reprogramming and STAM2 O-GlcNAcylation facilitate bladder cancer metastasis

Zhenwei Feng<sup>1,2</sup>, Yuhua Mei<sup>1,2</sup>, Haonan Chen<sup>1</sup>, Li Li<sup>1,2</sup>, Tian Jin<sup>1</sup>, Xinyuan Li<sup>1,2</sup>, Xin Gou<sup>1✉</sup> & Yong Chen<sup>1✉</sup>

Metabolic reprogramming and epigenetic alternations are implicated in tumor progression and metastasis, but the metabolic and epigenetic mechanisms underlying lymphatic and distant metastasis of bladder cancer (BCa) remain poorly understood. In this study, we provide the first evidence that glutamine-fructose-6-phosphate aminotransferase 1 (GFAT1), the crucial rate-limiting switch of the hexosamine biosynthesis pathway (HBP), is considerably upregulated in the nutrient-scarce microenvironment and causes a high O-GlcNAcylation of signal transducing adaptor molecule 2 (STAM2), further facilitating lymphatic and distant metastasis of BCa. Inhibition of GFAT1 and O-GlcNAcylation impairs STAM2-induced metastasis. Mechanistically, O-GlcNAcylation of STAM2 at serine 375 augments protein stability by inhibiting proteasome degradation and ubiquitination. In addition, STAM2 O-GlcNAcylation facilitates Janus kinase 2 (JAK2) and signal transducer and activator of transcription (STAT3) phosphorylation, thus activating the epithelial–mesenchymal transition. In summary, these results reveal a novel metabolic and epigenetic link mediating tumor metastasis, and indicate that targeting GFAT1 and STAM2 O-GlcNAcylation may serve as a promising treatment strategy for BCa progression.

**Keywords** STAM2, O-GlcNAcylation, Bladder cancer, Metastasis

Bladder cancer (BCa) is one of the most prevalent malignant tumors worldwide, with increasing morbidity and mortality rates<sup>1</sup>. Although surgical management and adjunctive therapy continue to progress, BCa recurrence rates remain high, which seriously affects patient survival and quality of life<sup>2–4</sup>. BCa recurrence is often attributed to the aggressive growth of residual tumor cells. However, rapidly growing cancer cells urgently need a large amount of nutrition from the tumor microenvironment (TME)<sup>5,6</sup>, while malformed tumor vascular networks cause starvation, which is characteristic of the TME<sup>7</sup>. Starvation strongly activates BCa cell function, triggering BCa cells metastasis and further promoting cancer progression<sup>8,9</sup>. Therefore, identifying novel treatment targets and mechanisms, with the consideration of the nutrient-deprived TME, seems to be important for BCa patients.

The hexosamine biosynthesis pathway (HBP) is a key branch of the glycolytic pathway, with glutamine-fructose-6-phosphate aminotransferase 1 (GFAT1) serving as the first and rate-limiting enzyme in this pathway<sup>10</sup>. Previous studies have revealed that inhibiting GFAT1 expression either by 6-diazo-5-oxo-L-norleucine (DON) or by siRNA-mediated knockdown significantly attenuated pancreatic cancer cell proliferation and metastasis<sup>11–13</sup>. In addition, the UDP-GlcNAc generated by GFAT1 can transfer GlcNAc to proteins for O-GlcNAcylation<sup>11,14,15</sup>. Recent evidence has shown that flux through the HBP and O-GlcNAc protein levels significantly increase in tumor cells, particularly under conditions of nutrient deprivation<sup>16,17</sup>. Our previous studies also demonstrated that starvation promotes the upregulation of GFAT1 and HBP in BCa cells<sup>13</sup>. Nevertheless, the role of starvation-mediated HBP-related metabolic reprogramming in BCa remains unclear.

In our study, we investigated the effect of metabolic reprogramming in the HBP mediated by starvation on the proliferation and metastasis of BCa cells. In addition, our findings reveal that starvation significantly increased HBP flux and O-GlcNAcylation by upregulating GFAT1 in BCa cells. Moreover, we present, for the first time, the functional importance of STAM2 O-GlcNAcylation in driving both proliferation and metastasis.

<sup>1</sup>Department of Urology, The First Affiliated Hospital of Chongqing Medical University, No.1 Youyi Road, Yuan Jiagang, Yuzhong District, Chongqing 400010, China. <sup>2</sup>Chongqing Key Laboratory of Molecular Oncology and Epigenetics, The First Affiliated Hospital of Chongqing Medical University, Chongqing 400016, China. ✉email: gouxincq@hospital.cqmu.edu.cn; tankcy@163.com

These results reveal a distinctive perspective on BCa metastasis mediated by starvation and imply that STAM2 is a potential therapeutic target for anticancer therapy.

## Methods

### Clinical samples

A total of 50 patients diagnosed with BCa who underwent tumor excision between June 2022 and July 2023 at the First Affiliated Hospital of Chongqing Medical University were included in the study. Patients with other primary and metastatic cancers were excluded. Tumor and adjacent normal tissues were collected for western blotting. Written informed consent was obtained from all participants. The study was approved by the Medical Ethics Committee of the First Affiliated Hospital of Chongqing Medical University (Approval No.2021–199) and was performed in accordance with all applicable guidelines and regulations. All clinical data were obtained by reviewing medical records.

### Animals

All the experiments were conducted in compliance with the Chongqing Medical University policy and in accordance with the guidelines and regulations. The animals study was approved by the university for the care and use of laboratory animals (Approval No.2021–277). All mice were humanely euthanized with pentobarbital sodium. This study was performed in accordance with the Animal Research: Reporting of In Vivo Experiments (ARRIVE) guidelines. All six-week-old female BALB/c nude mice and C57BL/6 mice were purchased from the Animal Center of Chongqing Medical University (Chongqing, CHN).

### Cell line-derived xenografts

Six-week-old female BALB/c nude mice were randomly divided into five groups, with three mice per group. A total of  $5 \times 10^6$  UM-UC-3 cells, treated as indicated and suspended in 100  $\mu$ l culture medium were subcutaneously inoculated into the right thigh roots of BALB/c nude mice. Tumor volume and body weight were monitored every 3 days for 21 days. Thiamet G (400  $\mu$ g/50  $\mu$ l normal saline) was injected peritumorally every 3 days. After 3 weeks, the mice were euthanized with pentobarbital sodium salt, and the tumors were collected, measured, and subjected to western blotting.

### Mouse model of popliteal lymphatic metastasis

Six-week-old C57BL/6 mice were randomly divided into three groups, with five mice per group. Briefly,  $1 \times 10^6$  luciferase-labeled MB-49 cells subjected to the indicated treatments were subcutaneously inoculated into the footpads of C57BL/6 mice. Luminescence of popliteal lymph nodes (LNs) was measured weekly using IVIS Lumina Series III (PerkinElmer, USA) until the footpad tumor size reached 200 mm<sup>3</sup>. The mice were subsequently sacrificed, and the popliteal LNs were measured and collected for further analysis.

### Tail vein injection

Four-week-old C57BL/6 mice were randomly divided into three groups, with five mice per group. Briefly,  $1 \times 10^6$  luciferase-labeled MB-49 cells subjected to the indicated treatments were intravenously injected into the tail vein of the mice. Three weeks after injection, the luminescence of the mice was measured via an IVIS Lumina Series III (PerkinElmer, USA).

### Cell culture

Human BCa cell lines (UM-UC-3, T24, and 5637), epithelial cell line SV-HUC-1, mouse BCa cell line MB-49, and HEK293T cells were purchased from the Cell Bank of the Chinese Academy of Sciences (Shanghai, CHN). The cell lines were tested for mycoplasma contamination. UM-UC3, T24, 5637, and SV-HUC-1 cells were cultured in Dulbecco's modified Eagle's medium (DMEM; Gibco, USA) supplemented with 10% fetal bovine serum (FBS, BioInd, Israel), 100  $\mu$ g/mL streptomycin (Beyotime, CHN), and 100 U/mL penicillin (Beyotime, CHN) at 37 °C in a humidified atmosphere of 5% CO<sub>2</sub>.

For nutrient-deprived cultures, UM-UC-3 cells were cultured in Hank's balanced salt solution (HBSS, Thermo Fisher Scientific, USA) for 6 to 24 h. Then, the HBSS was replaced with DMEM supplemented with 10% FBS.

### Cell transfection

STAM2-knockout cells were established using CRISPR-Cas9. The optimal small guide RNA (sgRNA) target sequence was GCAGATATCAGACTAAACTG, which was subsequently cloned and inserted into the PX458 plasmid. After that, lentiviral vectors (PLVX/EF1a/CMV/Puro) with STAM2-HA overexpression (OE STAM2) or STAM2 S375A-HA overexpression (OE STAM2 S375A-HA) were constructed through combination with related full-length cDNA fragments or specific cDNA fragments and then the above lentiviral vectors were transfected into UM-UC-3 and MB-49, followed by selection with puromycin (Hanbio, CHN) for 2 weeks.

### Quantitative real-time PCR (qRT–PCR)

Total RNA was extracted from tissues and cells using TRIzol Reagent (ABclonal, CHN) and reverse-transcribed to cDNA via ABScript Neo RT Master Mix for qPCR with gDNA Remover (ABclonal, CHN). qRT–PCR was conducted via SYBR Green Fast qPCR Mix (ABclonal, CHN) with a 7500 Real-Time PCR System (Thermo Fisher, USA). The 2– $\Delta$ CT method was used to calculate gene expression, which was normalized to that of the control group. The sequences of the primer pairs used were as follows: STAM2(forward:5'-AGGGCCTGAGTT GTTCCAAT-3', reverse:5'-AGGGGGAACATGAACAAGCAC-3');  $\beta$ -actin(forward: 5'-CCTTCCTGGGCATG GAGTC-3',reverse: 5'-TGATCTTCATTGTGCTGGGTG-3').

### Western blotting

Total cell protein was extracted using radioimmunoprecipitation (RIPA) lysis buffer (Beyotime, CHN) supplemented with protease inhibitors (Beyotime, CHN). Proteins were separated via sodium dodecyl sulfate-polyacrylamide gel electrophoresis (SDS-PAGE) and transferred to polyvinylidene difluoride (PVDF) membranes (Millipore, USA). The membranes were blocked with 5% fat-free milk (Beyotime, CHN) and subsequently incubated with primary antibodies at 4 °C overnight. The next day, the membranes were incubated with secondary antibodies (Bioss, CHN). A Fusion FX System (Vilber, Germany) was used to detect chemiluminescence signals, which were normalized to that of  $\beta$ -actin. The antibodies used in the study were as follows: STAM2 (Proteintech, 13009-1-AP), HA (Proteintech, 51064-2-AP), E-cadherin (Proteintech, 20874-1-AP), N-cadherin (Proteintech, 22018-1-AP), Vimentin (Proteintech, 10366-1-AP), JAK2 (CST, #3230), p-JAK2 (CST, #3771), stat3 (CST, #12640), p-stat3 (CST, #94994), and  $\beta$ -actin (Proteintech, 66009-1-Ig).

### STAM2 protein stability assay

UM-UC-3 cells were transfected with vectors expressing STAM2-HA or STAM2 S375A-HA and Ub-Flag. After cycloheximide was added to the culture medium for 0, 6, 12, or 24 h, proteins were extracted for western blot analysis using an anti-HA antibody.

### Immunofluorescence staining

The cells were fixed in 4% paraformaldehyde fixative (Beyotime, CHN) and permeabilized in Triton X-100 (Beyotime, CHN) for 10 min. After being blocked with 10% normal goat serum for 1 h, the cells were incubated with anti-HA and anti-Flag at 4 °C overnight. The following day, secondary antibodies were applied at room temperature for 1 h, and the cells were treated with antifade reagent containing DAPI for 10 min. Images were acquired using laser confocal microscopy at a magnification of 630x (LSCM, Leica Microsystems AG).

### Cell viability

According to the manufacturer's instructions, cell viability was assessed using Cell Counting Kit 8 (CCK-8, Dojindo, JPN). Briefly, 24 h after the intervention,  $2 \times 10^3$  cells were inoculated into a 96-well plate. A total of 90  $\mu$ l of serum-free, and 10  $\mu$ l of CCK-8 reagent were added to each well. After incubation at 37 °C for 1 h, the absorbance at 450 nm was measured via a microplate reader (Bio-Rad, USA).

### Migration and invasion assays

For the migration assays,  $3 \times 10^5$  cells resuspended in 200  $\mu$ l serum-free medium were inoculated into the upper Transwell chamber (Corning, USA). A total of 700  $\mu$ l of medium containing 10% FBS was added to the lower Transwell chamber, and the whole system was incubated at 37 °C in a humidified atmosphere of 5% CO<sub>2</sub> for 24 h. The cells were inoculated into a Transwell chamber coated with Matrigel for the invasion assays. Then, the cells were fixed in 4% paraformaldehyde fixative solution (Beyotime, CHN) and stained with 0.2% crystal violet. Eventually, the images were obtained via a digital camera system at a magnification of 200x and analyzed with ImageJ software (version 1.54f).

### Statistics

Statistical analyses were conducted using GraphPad Prism 9 (GraphPad Software, USA). The data are expressed as the means  $\pm$  standard deviations (SDs), and comparisons were performed using independent-sample t-tests and one-way ANOVA. A p-value of less than 0.05 was considered statistically significant.

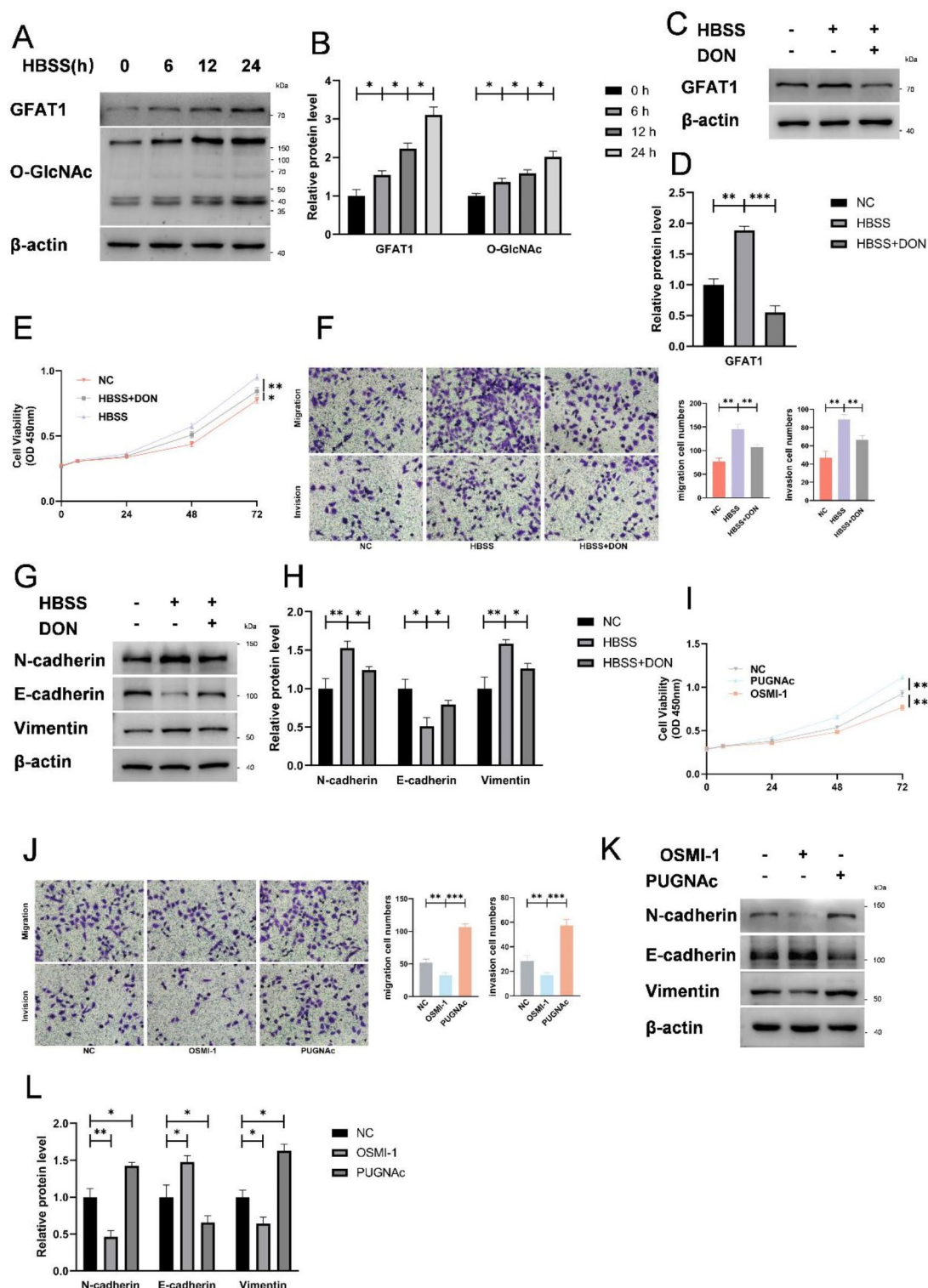
## Results

### A starvation microenvironment promotes proliferation, invasion, and migration by regulating GFAT1 in BCa cells

First, UM-UC-3 cells were cultured in a nutrient-deprived microenvironment, and we observed a marked increase in both GFAT1 expression and O-GlcNAcylation levels as starvation time increased (Fig. 1A–B). To explore the effect of starvation-induced upregulation of GFAT1 on the function of UM-UC-3, GFAT1 upregulation was reversed by DON, a GFAT1 inhibitor (Fig. 1C–D). Using functional assays, we found that starvation promoted the proliferation, migration, invasion, and epithelial-mesenchymal transition (EMT) of BCa cells. However, this starvation-mediated promotion was attenuated by DON (Fig. 1E–H). To further investigate whether the promoting effect of upregulated GFAT1 was mediated by O-GlcNAcylation, intracellular O-GlcNAcylation levels were modified using OSMI (an O-GlcNAc transferase inhibitor) and PUGNAc (an O-GlcNAcase inhibitor). Using CCK-8, cell migration, and Matrigel invasion assays, we found that the O-GlcNAcylation levels in UM-UC-3 cells were positively correlated with UM-UC-3 cell proliferation, migration, and invasion (Fig. 1I–L). These results suggest that the nutrient-deficient microenvironment mediates the increase in GFAT1 levels to promote BCa cell proliferation, migration, and invasion.

### STAM2 is upregulated in BCa cells and tissues

Our previous study suggested that STAM2 may be O-GlcNAcylated in a nutrient-deprived model<sup>13</sup>, so we further explored STAM2 in BCa. Compared with that in normal tissues, STAM2 expression was upregulated in BCa tissues (Fig. 2A–C). Additionally, STAM2 expression in human BCa cell lines (UM-UC-3, T24, and 5637) was also elevated compared with that in the normal bladder epithelial cell line SV-HUC-1 (Fig. 2D–F).



### A starvation microenvironment promotes proliferation, invasion, and migration by facilitating STAM2 O-GlcNAcylation

As shown in Fig. 3A, we demonstrated that STAM2 can be O-GlcNAcylated. The interaction between STAM2 and O-linked N-acetylglucosamine transferase (OGT) was confirmed using co-IP assays (Fig. 3B-C). Furthermore, starvation increased the O-GlcNAcylation level of STAM2 (Fig. 3D-E). To further investigate the function of STAM2 in a nutrient-scarce microenvironment, functional experiments were performed, demonstrating that the promoting effect of starvation on BCa cells in which STAM2 was knocked down was much weaker than that on normal control cells (Fig. 3F-I). To further explore the significance of STAM2 O-GlcNAcylation in UM-UC-3 cells, two potential O-GlcNAcylated sites, serine 372 (S372) and serine 375 (S375), were replaced with alanine (S372A, S375A). The results revealed that the O-GlcNAcylation level of STAM2 was significantly decreased at S375A (Fig. 3J-K), which suggested that serine 375 was the main O-GlcNAcylated site of STAM2.



◀ **Fig. 1.** A starvation microenvironment promotes proliferation, invasion, and migration by regulating GFAT1 in BCa cells. (A) GFAT1 and O-GlcNAc protein levels after time-incremental HBSS incubation in UM-UC-3 cells. (B) Quantitative western blot analysis of A. (C) GFAT1 protein levels in UM-UC-3 cells after 12 h of exposure to HBSS with or without DON. (D) Quantitative western blot analysis of C. (E) UM-UC-3 cell proliferation was measured by a CCK-8 assay after 12 h of exposure to HBSS with or without DON. (F) The migration and invasion of UM-UC-3 cells were measured by a CCK-8 assay after 12 h of exposure to HBSS with or without DON. (G) EMT marker protein levels were measured using western blotting after 12 h of exposure to HBSS with or without DON in UM-UC-3 cells. (H) Quantitative western blot analysis of the data in G. (I–J) Proliferation, migration, and invasion were measured using CCK-8 and Transwell assays after treatment with OSMI-1 or PUGNAc. (K) EMT marker protein levels were measured using western blotting after treatment with OSMI-1 or PUGNAc. (L) Quantitative western blot analysis of K. All PVDF bands were transferred and tested in the same western blot experiments. All the results are based on three distinct repetitions. Statistical significance is denoted as \*\*\* $p < 0.001$ , \*\* $p < 0.01$ , and \* $p < 0.05$ , indicating significant differences between two groups.

Finally, we explored the role of STAM2 S375 O-GlcNAcylation in proliferation, migration, invasion, and EMT. STAM2 promoted BCa cell proliferation, migration, and invasion, whereas the promoting effect of STAM2 S375A was weaker than that of STAM2 (Fig. 3L–O). More importantly, compared with the STAM2 + PUGNAc group, PUGNAc exhibited slight facilitative effects in the STAM2 S375A + PUGNAc group (Fig. 3L–O). These collective results indicate that starvation-mediated upregulation of STAM2 S375 O-GlcNAcylation improves the proliferation, migration, invasion, and EMT of UM-UC-3 cells.

### STAM2 S375 O-GlcNAcylation enhances its stability by decreasing ubiquitination

Next, we explored the specific mechanism by which STAM2 O-GlcNAcylation impacts UM-UC-3 cells. Previous studies have demonstrated that O-GlcNAcylation can regulate protein stability and localization<sup>18–20</sup>. Therefore, we used the cycloheximide (CHX) chase assays to detect STAM2 protein stability. As shown in Fig. 4A and B, enhancing of STAM2 O-GlcNAcylation with PUGNAc significantly prolonged the half-life of STAM2, whereas inhibiting STAM2 O-GlcNAcylation with OSMI-1 significantly shortened the half-life of STAM2. In addition, the impact of PUGNAc and OSMI-1 on the half-life of STAM2 was considerably reduced when the main O-GlcNAcylation site (serine 375) on STAM2 was mutated (Fig. 4C–D). These findings suggest that S375 O-GlcNAcylation of STAM2 enhances its stability. To further investigate how STAM2 O-GlcNAcylation contributes to its stability, we detected the proteasomal degradation of STAM2. We found that PUGNAc weakened the interaction between ubiquitin and STAM2, whereas OSMI-1 had the opposite effect (Fig. 4E–F). Furthermore, no significant difference in the interaction between ubiquitin and S375A STAM2 was noted when the cells were treated with PUGNAc or OSMI-1 (Fig. 4G–H). These results indicate that STAM2 O-GlcNAcylation stabilizes STAM2 by inhibiting its proteasome degradation. In addition, we further investigated the effect of STAM2 O-GlcNAcylation on protein localization using immunofluorescence assays. As shown in Fig. 4I, STAM2 was located mainly in the cytoplasm. However, STAM2 nuclear levels did not notably increase after O-GlcNAcylation was modified by PUGNAc or OSMI-1 (Fig. 4I–J), suggesting that STAM2 O-GlcNAcylation did not affect its localization. Building on these findings, we propose that starvation-mediated upregulation of STAM2 O-GlcNAcylation enhances its stability by decreasing its degree of ubiquitination.

### STAM2 S375 O-GlcNAcylation facilitates the JAK2–STAT3 signaling pathway

Previous studies have shown that STAM2 is involved in the JAK–STAT pathway<sup>21,22</sup>. Therefore, we detected the impact of STAM2 on the JAK2–STAT3 pathway by western blotting. First, we established STAM2 knockout (KO STAM2) or STAM2 overexpression (OE STAM2) cell line and validated using western blotting (Fig. 5A). The results showed that overexpression of STAM2 increased phospho-JAK2 (p-JAK2) and phospho-STAT3 (p-STAT3) levels, whereas knockout of STAM2 had the opposite effect (Fig. 5B–C). In addition, the STAM2-overexpressing group presented higher p-JAK2 and p-STAT3 levels than the OE STAM2 S375A group did (Fig. 5D–E). Furthermore, compared with the STAM2 S375A + PUGNAc group, PUGNAc significantly promoted p-JAK2 and p-STAT3 expression in the STAM2 + PUGNAc group (Fig. 5D–E). Moreover, rescue experiments revealed that JSI-124, a selective inhibitor of JAK2–STAT3, reduced the proliferation, migration, invasion, and EMT of UM-UC-3 cells. Moreover, STAM2 overexpression counteracted the suppressive effects of JSI-124 on BCa cells, whereas STAM2 375 A overexpression partially reversed the suppressive effects (Fig. 5F–I).

### STAM2 S375 O-GlcNAcylation promotes tumor proliferation and metastasis in vivo

To further validate the role of STAM2 O-GlcNAcylation, we knocked out endogenous STAM2 in UM-UC3 cells and re-expressed them with lentiviral vectors (pLVX/EF1a/CMV/Puro) carrying STAM2 or STAM2 S375A. Next, we established a subcutaneous xenograft model in nude mice (Fig. 6A). We found that tumors re-expressing STAM2 S375A were smaller than those re-expressing STAM2 (Fig. 6B–D). In addition, PUGNAc significantly accelerated tumor growth in cells re-expressing with STAM2 but not in cells re-expressing STAM2 S375A (Fig. 6B–D). Additionally, we detected the expression levels of EMT marker as well as the phosphorylation levels of JAK2 and STAT3 in tumor tissues using Western blotting. We found that the group with higher p-JAK2 and p-STAT3 levels also presented higher N-cadherin and vimentin expression levels, alongside reduced E-cadherin levels (Fig. 6E–H). To further demonstrate the role of STAM2 in metastasis, we constructed stable MB49 cells with luciferase-labeled STAM2 or STAM2 S375A. Using a lung metastasis model, we found that the lung bioluminescent signals were stronger in the STAM2 group than in the STAM2 S375A group (Fig. 6I–J).

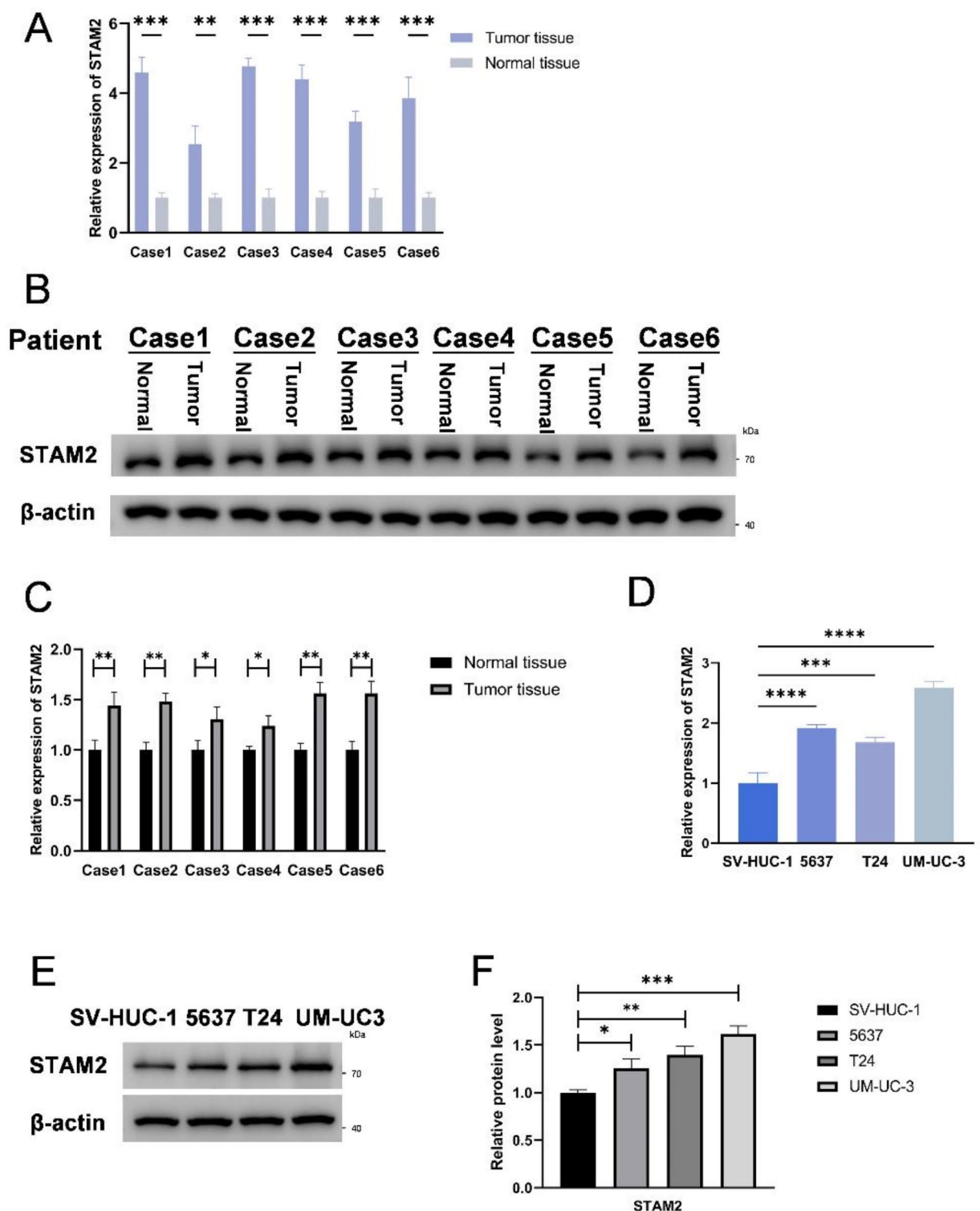


**Fig. 2.** STAM2 is upregulated in BCa cells and tissues. (**A–B**) STAM2 mRNA and protein levels were detected using qRT-PCR and western blotting in tumor tissues and adjacent normal tissues. **C** Quantitative western blot analysis of the data in **B**. (**D–E**) STAM2 mRNA and protein levels were detected using qRT-PCR and western blotting in an epithelial cell line (SV-HUC-1) and BCa cell lines (UM-UC-3, T24, and 5637). (**F**) Quantitative western blot analysis of **E**. (All PVDF bands were transferred and tested in the same western blot experiments, and the experiments performed in triplicate.)

Additionally, in the popliteal lymphatic metastasis model, we found that the STAM2 group presented stronger bioluminescence signals in the popliteal lymph nodes (Fig. 6K–N), and larger popliteal lymph nodes than the STAM2 S375A group did (Fig. 6K–N). These results suggest that STAM2 O-GlcNAcylation may be crucial for BCa progression.

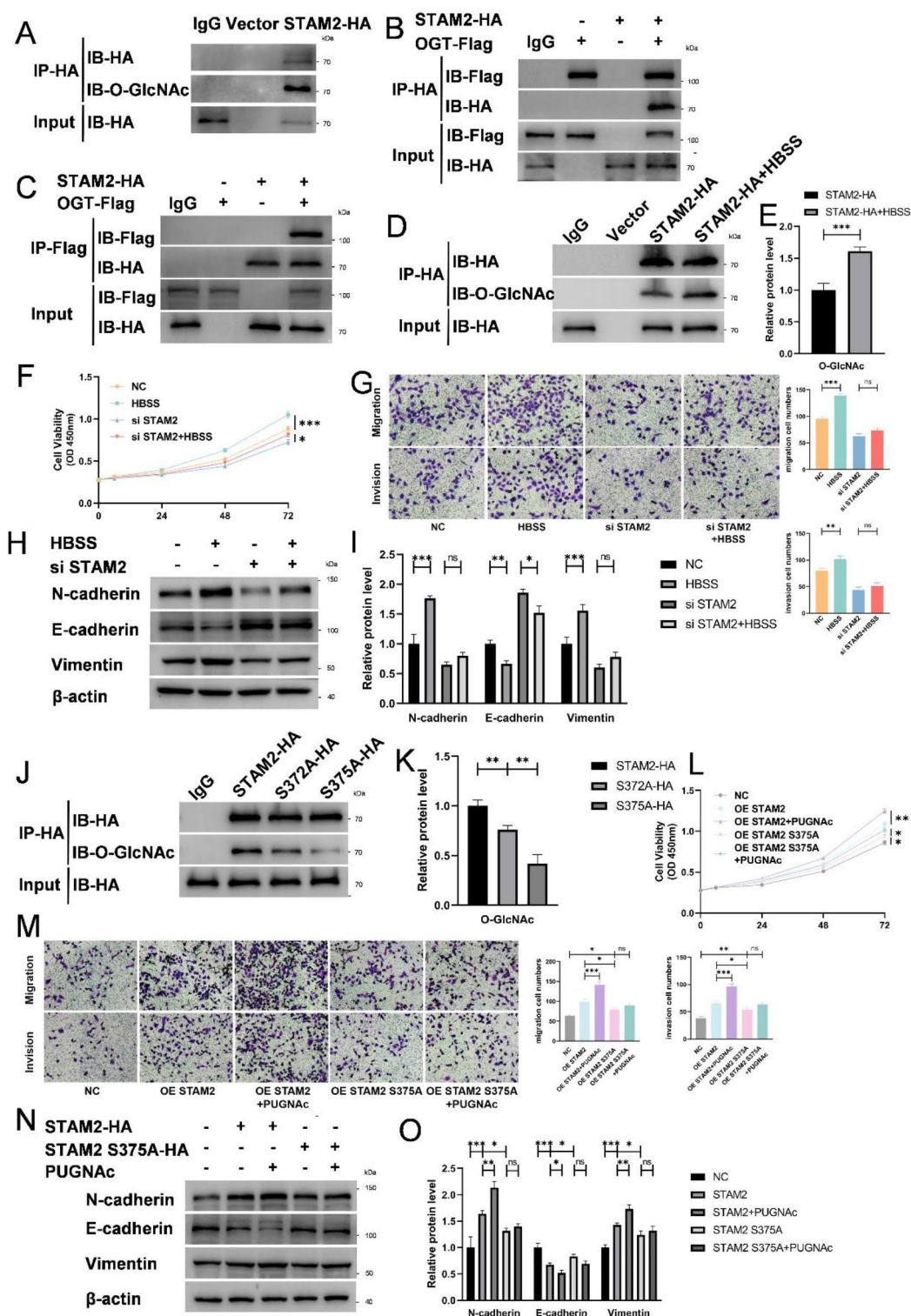
## Discussion

The microenvironment in solid tumors is thought to be nutrient-deprived<sup>23</sup>, which significantly impacts tumor growth and progression. In the context of an unstable nutrient supply and repeated starvation, tumor cells rapidly reprogram metabolism and biological behaviors using intracellular signals<sup>24,25</sup>. Accumulating evidence has demonstrated that HBP flux promotes tumor progression<sup>26–28</sup>. Previous studies have shown that starvation induces the upregulation of GFAT1<sup>16,29</sup> and that upregulated GFAT1 inhibits cell apoptosis under starvation<sup>30</sup>. However, the potential mechanisms by which starvation induces GFAT1-regulated BCa cells remain poorly understood. Here, we demonstrate that starvation-mediated upregulation of GFAT1 and, accordingly, increased protein O-GlcNAcylation levels in BCa cells promote BCa proliferation, migration, invasion, and EMT.

Increasing evidence suggests that a high level of O-GlcNAcylation is a common feature of various cancers, such as BCa, breast cancer, and prostate cancer<sup>31–33</sup>, and is closely related to tumor proliferation<sup>34</sup> and metastasis<sup>35</sup>. However, few studies have assessed O-GlcNAcylation in BCa. A recent study by Hye Won Li demonstrated that depressed OGT and, accordingly, decreased protein O-GlcNAcylation levels attenuate proliferation, invasion, migration, and drug resistance in BCa<sup>36</sup>. However, the specific O-GlcNAc proteins that affect BCa remain unclear. Our study revealed that STAM2 can be O-GlcNAc at serine 372 and serine 375 in BCa cells. In addition, starvation-induced upregulation of O-GlcNAcylation of STAM2 promotes the proliferation, invasion, and migration of BCa cells.

STAM2, a member of the endosomal sorting complex required for transport (ESCRT – 0)<sup>37</sup>, plays a vital role in signal transduction and recognition of ubiquitinated receptors. Previous studies have shown that STAM2 is involved in signal transduction mediated by cytokines and growth factors, such as epidermal growth factor and platelet-derived growth factor<sup>38,39</sup>, and is associated with the JAK2–STAT3 signaling pathway<sup>22</sup>. Yang Yang and colleagues suggested that STAM2 is significantly overexpressed in gastric cancer and that high STAM2 expression is associated with proliferation, metastasis, and poor prognosis<sup>22</sup>. In addition, STAM2 knockdown inhibited the JAK2–STAT3 signaling pathway in gastric cancer cells. Our study further revealed that STAM2 O-GlcNAcylation promotes JAK2 and STAT3 phosphorylation, thereby promoting proliferation, migration, invasion, and EMT in BCa. Mechanistically, STAM2 O-GlcNAcylation stabilizes STAM2 by inhibiting its proteasome degradation. Furthermore, STAM2 is localized mainly in the cytoplasm and partially in the nucleus in BCa cells, and O-GlcNAcylation has no significant effect on its localization. However, previous studies have shown that STAM2 is predominantly localized in the nucleus of neuronal cells, indicating that STAM2 may play an additional role in signal transduction. The impact of STAM2 O-GlcNAcylation on its own phosphorylation was not further elucidated in our study. The exact molecular interactions of STAM2 O-GlcNAcylation with JAK2 and STAT3 will be a significant focus of our future studies.

Overall, our results suggest that starvation-mediated upregulation of GFAT1 in BCa cells promotes STAM2 O-GlcNAcylation. The O-GlcNAcylation of STAM2 promotes the JAK2–STAT3 signaling pathway by increasing its stability, which facilitates the proliferation, migration, invasion, and EMT of BCa cells under starvation conditions. The present study provides new perspectives on the role of HBP metabolism in BCa cells in the starvation microenvironment. These findings increase our understanding of the ability of starvation-mediated STAM2 O-GlcNAcylation to promote tumor metastasis, which may provide potential targets for BCa therapy.





◀ **Fig. 3.** A starvation microenvironment promotes proliferation, invasion, and migration by facilitating STAM2 O-GlcNAcylation. **(A)** STAM2 IP assay was conducted in UM-UC-3 cells transfected with either STAM2-HA or vector. STAM2-HA and O-GlcNAc were detected using the indicated antibodies. **(B–C)** Co-IP assays validated the interaction between STAM2-HA and OGT-Flag using anti-HA **(B)** or anti-Flag **(C)** antibodies. **(D)** STAM2 IP assay in UM-UC-3 cells transfected with STAM2-HA or vector (HBSS incubation for 12 h). **(E)** Quantitative western blot analysis of STAM2 O-GlcNAcylation. **(F–G)** Proliferation, migration, and invasion were measured using CCK-8 and Transwell assays. **(H)** EMT marker protein levels were measured using western blot. **(I)** Quantitative western blot analysis of H. **(J)** STAM2 O-GlcNAcylation was detected via an IP assay in UM-UC-3 cells transfected with STAM2-HA, STAM2 S372-HA, or STAM2 S375-HA. **(K)** Quantitative western blot analysis of STAM2 O-GlcNAcylation. **(L–M)** Proliferation, migration, and invasion were measured using CCK-8 and Transwell assays. **(N)** EMT marker protein levels were measured using western blotting. **(O)** Quantitative western blot analysis of N. All PVDF bands were transferred and tested in the same western blot experiments. All the results are based on three distinct repetitions. Statistical significance is denoted as \*\*\* $p < 0.001$ , \*\* $p < 0.01$ , and \* $p < 0.05$ , indicating significant differences between two groups.

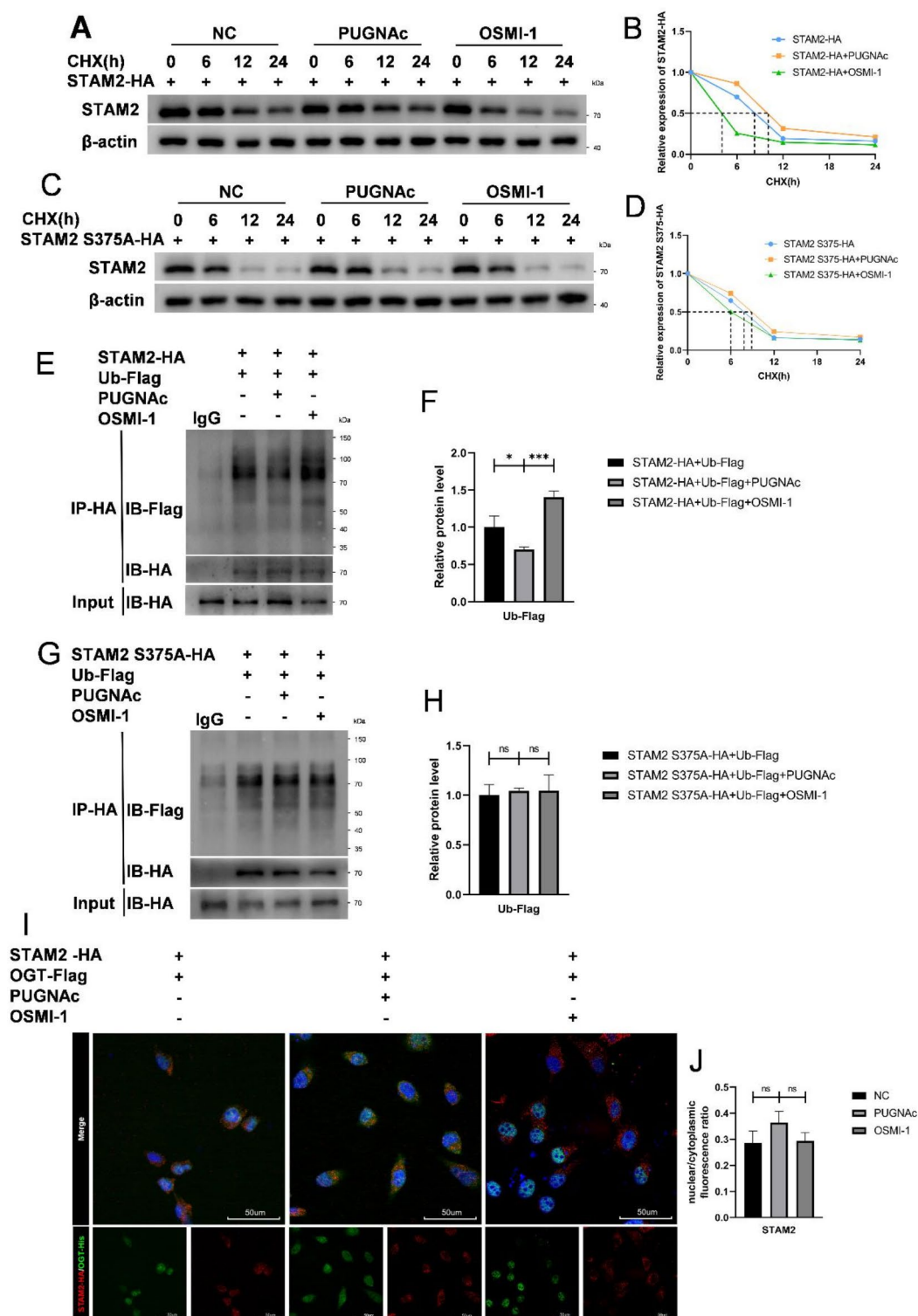


**Fig. 4.** STAM2 S375 O-GlcNAcylation enhances its stability by decreasing ubiquitination. Half-life and quantitative analysis of STAM2-HA (A–B) and STAM2 S375A-HA (C–D) in UM-UC-3 cells. E Co-IP assays detected the interaction between STAM2-HA and Ub-Flag in UM-UC-3 cells transfected with STAM2-HA. (F) Quantitative western blot analysis of ubiquitination. (G) Co-IP assays detected the interaction between STAM2-HA and Ub-Flag in UM-UC-3 cells transfected with STAM2 S375A-HA. (H) Quantitative western blot analysis of ubiquitination. (I) Immunofluorescence staining of STAM2-HA and OGT-Flag in UM-UC-3 cells treated with OSMI-1 or PUGNAc. (J) Quantification of the nuclear/cytoplasmic fluorescence ratios of STAM2. (All PVDF bands were transferred and tested in the same western blot experiments, and the experiments performed in triplicate.)

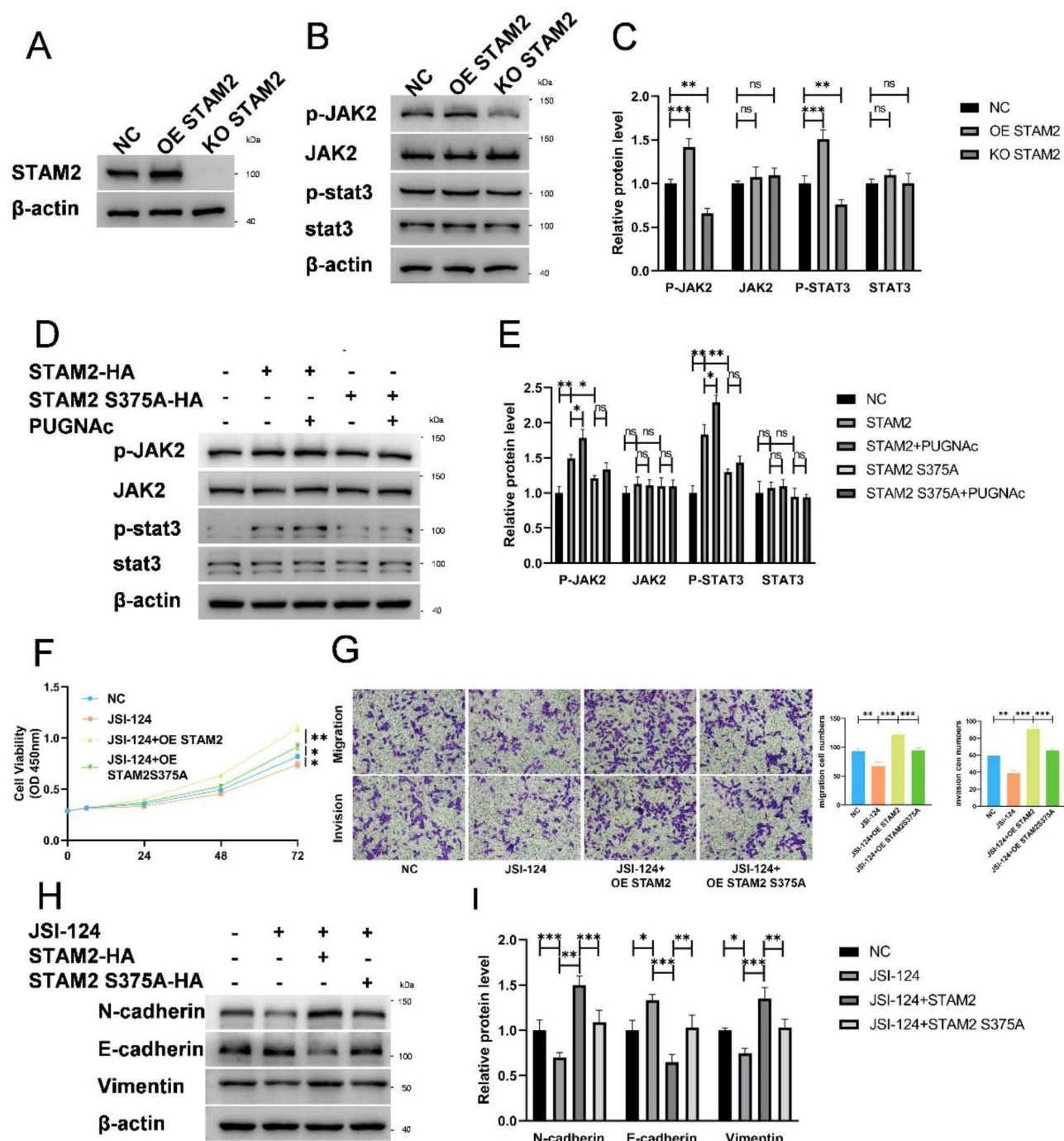


**Fig. 5.** STAM2 S375 O-GlcNAcylation facilitates the JAK2-STAT3 signaling pathway. **(A)** STAM2 protein levels were measured using western blotting. **(B)** JAK2/p-JAK2 and STAT3/p-STAT3 protein levels were measured using western blotting in NC cells, STAM2-overexpressing cells and STAM2-knockout cells. **(C)** Quantitative western blot analysis of B. **(D)** JAK2/p-JAK2 and STAT3/p-STAT3 protein levels were measured using western blot in UM-UC-3 cells transfected with STAM2-HA or STAM2 S375A-HA and treated with PUGNAc or not. **(E)** Quantitative western blot analysis of D. **(F-G)** Proliferation, migration, and invasion were measured using CCK-8 and Transwell assays in NC cells or cells transfected with STAM2-HA or STAM2 S375A-HA after treatment with JSI-124. **(H)** EMT marker protein levels were measured using western blotting. **(I)** Quantitative western blot analysis of H. All PVDF bands were transferred and tested in the same western blot experiments. All the results represent three distinct repetitions. Statistical significance is denoted as \*\*\* $p$  < 0.001, \*\* $p$  < 0.01, and \* $p$  < 0.05, indicating significant differences between two groups.

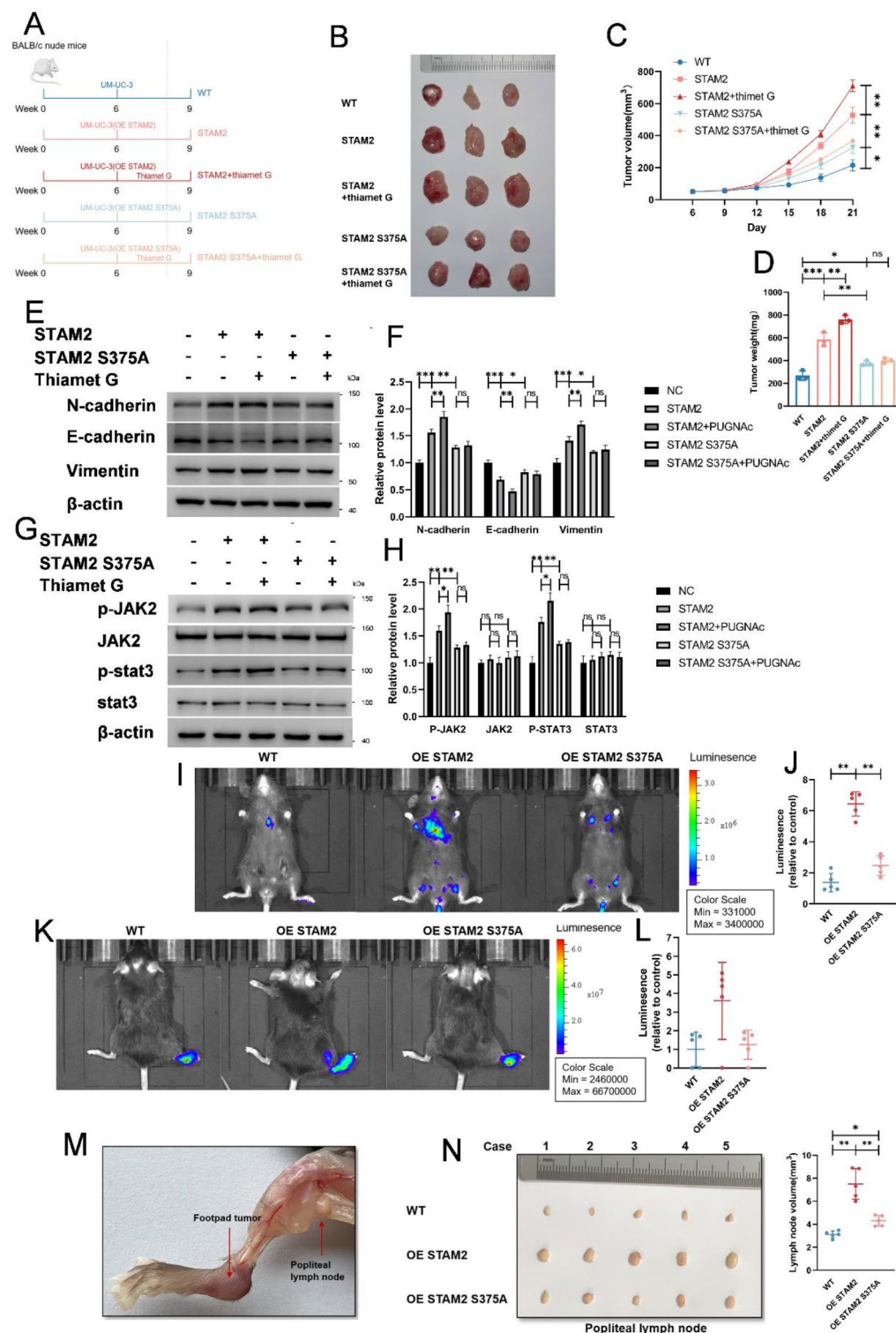


**Fig. 6.** STAM2 S375 O-GlcNAcylation promotes tumor proliferation and metastasis in vivo. **(A)** Schematic representation of the establishment of UM-UC-3-derived xenografts. **(B)** Representative images of xenograft tumors 21 days after subcutaneous injection. **(C)** Tumor volumes were measured every 3 days. **(D)** Weights of xenograft tumors 21 days after subcutaneous injection. **(E–H)** Protein levels of EMT marker JAK2/p-JAK2 and STAT3/p-STAT3 were measured using western blotting. All PVDF bands were transferred and tested in the same western blot experiments, and the experiments performed in triplicate. **(I–L)** Bioluminescence detection and bioluminescence quantitative analysis of the lung **(I–J)** and popliteal lymph nodes **(K–L)**. **(M–N)** Representative image of the popliteal lymphatic metastasis model, along with quantitative analysis of the volume of popliteal lymph nodes.



## Data availability

All data of the study are available on reasonable requirements from the corresponding author.

Received: 2 December 2024; Accepted: 28 February 2025

Published online: 12 March 2025

## References

1. Rebecca, L. S., Angela, N. G. & Ahmedin, J. Cancer statistics, 2024. *CA Cancer J. Clin.*, **74**(1). (2024).
2. Bas, W. G. V. R. et al. Recurrence and progression of disease in non-muscle-invasive bladder cancer: from epidemiology to treatment strategy. *Eur. Urol.*, **56**(3). (2009).
3. Fei, L. et al. FGFBP1 as a potential biomarker predicting bacillus Calmette-Guérin response in bladder cancer. *Front. Immunol.*, **13**(0). (2022).
4. James, W. F. C. et al. Quality of life after bladder cancer: A Cross-sectional survey of patient-reported outcomes. *Eur. Urol.*, **79**(5). (2021).
5. Douglas, H. & Robert, A. W. Hallmarks of cancer: the next generation. *Cell*, **144**(5). (2011).
6. Tianjian, Y. & Genhong, D. Role of tumor microenvironment in triple-negative breast cancer and its prognostic significance. *Chin. J. Cancer Res.*, **29**(3). (2017).
7. Ueda, Y. et al. Glioma cells under hypoxic conditions block the brain microvascular endothelial cell death induced by serum starvation. *J. Neurochem.* **95** (1), 99–110 (2005).
8. Li, T. et al. Starvation induced autophagy promotes the progression of bladder cancer by LDHA mediated metabolic reprogramming. *Cancer Cell Int.*, **21**(1). (2021).
9. Tong, H. et al. Starvation-induced autophagy promotes the invasion and migration of human bladder cancer cells via TGF- $\beta$ 1/Smad3-mediated epithelial-mesenchymal transition activation. *J. Cell. Biochem.* **120** (4), 5118–5127 (2019).
10. Lam, C. et al. The hexosamine biosynthetic pathway and cancer: current knowledge and future therapeutic strategies. *Cancer Lett.* **503**, 11–18 (2021).
11. Sharma, N. S. et al. Targeting tumor-intrinsic hexosamine biosynthesis sensitizes pancreatic cancer to anti-PD1 therapy. *J. Clin. Invest.* **130** (1), 451–465 (2020).
12. Kim, P. K. et al. Hyaluronic acid fuels pancreatic cancer cell growth. *Elife*, **10**. (2021).
13. Li, X. et al. Bladder Cancer-Derived small extracellular vesicles promote tumor angiogenesis by inducing HBP-Related metabolic reprogramming and SerRS O-GlcNAcylation in endothelial cells. *Adv. Sci.*, **9**(30). (2022).
14. Coussement, P. et al. Mapping and refactoring pathway control through metabolic and protein engineering: the hexosamine biosynthesis pathway. *Biotechnol. Adv.*, **40**. (2020).
15. Olson, A. K. et al. First characterization of glucose flux through the hexosamine biosynthesis pathway (HBP) in *ex vivo* mouse heart. *J. Biol. Chem.* **295** (7), 2018–2033 (2020).
16. Moloughney, J. G. et al. mTORC2 modulates the amplitude and duration of GFAT1 Ser-243 phosphorylation to maintain flux through the hexosamine pathway during starvation. *J. Biol. Chem.* **293** (42), 16464–16478 (2018).
17. Palorini, R. et al. Glucose Starvation Induces Cell Death in K-ras-transformed Cells by Interfering With the Hexosamine Biosynthesis Pathway and Activating the Unfolded Protein response4 (Cell Death & Disease, 2013).
18. Duan, F. et al. O-GlcNAcylation of RACK1 promotes hepatocellular carcinogenesis. *J. Hepatol.* **68** (6), 1191–1202 (2018).
19. Yan, W. et al. Cancer-cell-secreted miR-122 suppresses *in vivo* O-GlcNAcylation to promote skeletal muscle proteolysis. *Nat. Cell Biol.* **24** (5), 793– (2022).
20. He, X. et al. O-GlcNAcylation and stabilization of SIRT7 promote pancreatic cancer progression by blocking the SIRT7-REGLY interaction. *Cell Death Differ.* **29** (10), 1970–1981 (2022).
21. Endo, K. et al. STAM2, a new member of the STAM family, binding to the Janus kinases. *FEBS Lett.* **477** (1–2), 55–61 (2000).
22. Yang, Y. et al. STAM2 knockdown inhibits proliferation, migration, and invasion by affecting the JAK2/STAT3 signaling pathway in gastric cancer. *Acta Biochim. Biophys. Sin.* **53** (6), 697–706 (2021).
23. Grasmann, G. et al. Gluconeogenesis in cancer cells - repurposing of a starvation-induced metabolic pathway?. *Biochim. Et Biophys. Acta-Reviews Cancer.* **1872** (1), 24–36 (2019).
24. Buono, R., Longo, V. D. & Starvation stress resistance, and Cancer. *Trends Endocrinol. Metab.* **29** (4), 271–280 (2018).
25. Dart, A. Starving tumours. *Nat. Rev. Cancer.* **20** (3), 141–141 (2020).
26. Munemoto, M. et al. Roles of the hexosamine biosynthetic pathway and Pentose phosphate pathway in bile acid-induced cancer development. *Cancer Sci.* **110** (8), 2408–2420 (2019).
27. Liu, Y. et al. O-GlcNAc elevation through activation of the hexosamine biosynthetic pathway enhances cancer Cell chemoresistance9 (Cell Death & Disease, 2018).
28. Ricciardiello, F. et al. Inhibition of the hexosamine biosynthetic pathway by targeting PGM3 causes breast cancer growth arrest and apoptosis9 (Cell Death & Disease, 2018).
29. Moloughney, J. G. et al. mTORC2 responds to glutamine catabolite levels to modulate the hexosamine biosynthesis enzyme GFAT1. *Mol. Cell.* **63** (5), 811–826 (2016).
30. Wei, S. et al. GFAT1-linked Table 1 glutamylation sustains p38 MAPK activation and promotes lung cancer cell survival under glucose starvation. *Cell. Discovery*, **8**(1). (2022).
31. Liu, Y. et al. FOXA1 O-GlcNAcylation-mediated transcriptional switch governs metastasis capacity in breast cancer. *Sci. Adv.*, **9**(33). (2023).
32. Makwana, V., Rudrawar, S. & Anoopkumar-Dukie, S. Signalling Transduction of *in vivo* O-GlcNAcylation and PI3K/AKT/mTOR-axis in Prostate cancer1867 (Biochimica Et Biophysica Acta-Molecular Basis of Disease, 2021). 7.
33. Jin, L. et al. Blockage of O-linked GlcNAcylation Induces AMPK-dependent autophagy in bladder cancer cells25 (Cellular & Molecular Biology Letters, 2020). 1.
34. Zhu, Q. et al. O-GlcNAcylation promotes pancreatic tumor growth by regulating malate dehydrogenase 1. *Nat. Chem. Biol.* **18** (10), 1087– (2022).
35. Huang, H. et al. O-GlcNAcylation promotes the migratory ability of hepatocellular carcinoma cells via regulating FOXA2 stability and transcriptional activity. *J. Cell. Physiol.* **236** (11), 7491–7503 (2021).
36. Lee, H. W. et al. Targeted Inhibition of O-Linked  $\beta$ -N-Acetylglucosamine transferase as a promising therapeutic strategy to restore chemosensitivity and attenuate aggressive tumor traits in chemoresistant urothelial carcinoma of the bladder. *Biomedicines*, **10**(5). (2022).
37. Mizuno, E. et al. Association with Hrs is required for the early endosomal localization, stability, and function of STAM. *J. BioChem.* **135** (3), 385–396 (2004).
38. Takeshita, T. et al. STAM, signal transducing adaptor molecule, is associated with Janus kinases and involved in signaling for cell growth and c-myc induction. *Immunity* **6** (4), 449–457 (1997).
39. Takeshita, T. et al. Cloning of a novel signal-transducing adaptor molecule containing an SH3 domain and ITAM. *Biochem. Biophys. Res. Commun.* **225** (3), 1035–1039 (1996).

## Author contributions

Zhenwei Feng wrote the paper and prepared Figs. 1, 2, 3 and 4. Yuhua Mei and Haonan Chen performed most parts of the experiments in Figs. 5 and 6. Li Li and Tian Jin analyzed the data. Xinyuan Li collected clinical samples used in Fig. 2. Xin Gou and Yong Chen designed the study and revised the paper.

## Declarations

### Competing interests

The authors declare no competing interests.

### Ethics committee approval and patient consent

Written informed consent was obtained from all participants, and the study received approval from the Medical Ethics Committee of the First Affiliated Hospital of Chongqing Medical University (Approval No. 2021 – 199).

### Additional information

**Supplementary Information** The online version contains supplementary material available at <https://doi.org/10.1038/s41598-025-92579-4>.

**Correspondence** and requests for materials should be addressed to X.G. or Y.C.

**Reprints and permissions information** is available at [www.nature.com/reprints](http://www.nature.com/reprints).

**Publisher's note** Springer Nature remains neutral with regard to jurisdictional claims in published maps and institutional affiliations.

**Open Access** This article is licensed under a Creative Commons Attribution-NonCommercial-NoDerivatives 4.0 International License, which permits any non-commercial use, sharing, distribution and reproduction in any medium or format, as long as you give appropriate credit to the original author(s) and the source, provide a link to the Creative Commons licence, and indicate if you modified the licensed material. You do not have permission under this licence to share adapted material derived from this article or parts of it. The images or other third party material in this article are included in the article's Creative Commons licence, unless indicated otherwise in a credit line to the material. If material is not included in the article's Creative Commons licence and your intended use is not permitted by statutory regulation or exceeds the permitted use, you will need to obtain permission directly from the copyright holder. To view a copy of this licence, visit <http://creativecommons.org/licenses/by-nc-nd/4.0/>.

© The Author(s) 2025